APPLIED SCIENCES AND ENGINEERING

Electrothermal soft manipulator enabling safe transport and handling of thin cell/tissue sheets and bioelectronic devices

Byoung Soo Kim[1]*, Min Ku Kim[2]*, Younghak Cho[3], Eman E. Hamed[4], Martha U. Gillette[4,5], Hyeongyun Cha[6,7], Nenad Miljkovic[6,7,8,9], Vinay K. Aakalu[10], Kai Kang[10], Kyung-No Son[10], Kyle M. Schachtschneider[11,12,13], Lawrence B. Schook[11,12], Chenfei Hu[9], Gabriel Popescu[9], Yeonsoo Park[2], William C. Ballance[1], Seunggun Yu[14], Sung Gap Im[3], Jonghwi Lee[15†], Chi Hwan Lee[2,16†], Hyunjoon Kong[1,5,17†]

"Living" cell sheets or bioelectronic chips have great potentials to improve the quality of diagnostics and therapies. However, handling these thin and delicate materials remains a grand challenge because the external force applied for gripping and releasing can easily deform or damage the materials. This study presents a soft manipulator that can manipulate and transport cell/tissue sheets and ultrathin wearable biosensing devices seamlessly by recapitulating how a cephalopod's suction cup works. The soft manipulator consists of an ultrafast thermo-responsive, microchanneled hydrogel layer with tissue-like softness and an electric heater layer. The electric current to the manipulator drives microchannels of the gel to shrink/expand and results in a pressure change through the microchannels. The manipulator can lift/detach an object within 10 s and can be used repeatedly over 50 times. This soft manipulator would be highly useful for safe and reliable assembly and implantation of therapeutic cell/tissue sheets and biosensing devices.

INTRODUCTION

Over the past decade, there have been great successes in assembling high-performance biological and electronic materials with thin and sophisticated architecture. For example, monolayered cell sheets have shown to reproduce physiological activities of original tissue and exhibit enhanced therapeutic efficacy than individual cells because of increased cell-cell interactions and the presence of an extracellular matrix (*1*–*4*). These cell sheets are being studied extensively to assemble in vitro disease models and treat wounded or defective tissues and organs. Separately, minimizing the thickness of wearable electronic devices enables conformal adhesion without an interfacial gap and, in turn, improves performance for sensing, diagnosis, and therapies (*5*–*8*). However, handling such delicate and thin materials for transport and assembly remains a grand challenge. External forces used for gripping, holding, and discharging such materials often deform, wrinkle, or damage materials (*9*). Such damage can be avoided by attaching thin materials to sacrificial polymeric supports including water-soluble or thermal release tapes (*10*–*12*). However, these supports should be removed with chemical or long-lasting heat treatment following the placement of thin materials onto a target site, thus making them not reusable.

Recently, efforts have emerged to transport thin electronic materials by simulating the ability of cephalopods (e.g., octopus and squid) to capture and release their preys (*13*–*15*). Cephalopods use many muscle-based suction cups, called suckers, on their arms to attain conformal adhesion to target preys in both wet and dried environments (*16*, *17*). Bioelectrical signals control the rapid contraction and relaxation of the soft muscle and, in turn, change the internal pressure of the suckers. However, most material-handling systems that were devised to mimic the suction cups focus on recapitulating the anatomical structure but overlook the roles of the bioelectrical signal for control. Therefore, these strategies require mechanical force to be applied externally to attach and detach materials of interests. In addition, synthetic suction cups made with polydimethylsiloxane (PDMS) or polyurethane acrylates are more rigid than biological suction cups by two or three orders of magnitude (*13*, *15*). Such rigid suction cups require higher external pressure for gripping than biological ones, thus increasing the possibility to damage thin and soft materials. Certain efforts were made to assemble a device that can hold and detach materials with heat by coating porous PDMS with thermally responsive poly(*N*-isopropyl acrylamide) (PNIPAAm) (*14*). However, the manipulation process was only possible while submerged in a water bath. In addition, it takes

[1]Department of Chemical and Biomolecular Engineering, University of Illinois at Urbana-Champaign, Urbana, IL 61801, USA. [2]Weldon School of Biomedical Engineering, Purdue University, West Lafayette, IN 47907, USA. [3]Department of Chemical and Biomolecular Engineering, Korea Advanced Institute of Science and Technology, Daejeon 34141, Republic of Korea. [4]Neuroscience Program, Beckman Institute for Advanced Science & Technology, University of Illinois at Urbana-Champaign, Urbana, IL 61801, USA. [5]Department of Bioengineering, Institute for Genomic Biology, University of Illinois at Urbana-Champaign, Urbana, IL 61801, USA. [6]Department of Mechanical Science and Engineering, University of Illinois at Urbana-Champaign, Urbana, IL 61801, USA. [7]International Institute for Carbon Neutral Energy Research, Kyushu University, Nishi-ku, Fukuoka 819-0395, Japan. [8]Materials Research Laboratory, University of Illinois at Urbana-Champaign, Urbana, IL 61801, USA. [9]Department of Electrical and Computer Engineering, University of Illinois at Urbana-Champaign, Urbana, IL 61801, USA. [10]Illinois Eye and Ear Infirmary, University of Illinois College of Medicine at Chicago, Chicago, IL 60612, USA. [11]Department of Radiology, University of Chicago, Chicago, IL 60612, USA. [12]National Center for Supercomputing Applications, University of Illinois at Urbana-Champaign, Urbana, IL 61801, USA. [13]Department of Biochemistry and Molecular Genetics, University of Chicago, Chicago, IL 60612, USA. [14]Insulation Materials Research Center, Korea Electrotechnology Research Institute (KERI), Changwon 51543, Republic of Korea. [15]Department of Chemical Engineering and Materials Science, Chung-Ang University, Seoul 06974, Republic of Korea. [16]School of Mechanical Engineering, Purdue University, West Lafayette, IN 47907, USA. [17]Department of Medical Engineering, College of Medicine, Yonsei University, Seoul 03722, Republic of Korea.
*These authors contributed equally to this work.
†Corresponding author. Email: hjkong06@illinois.edu (H.K.); lee2270@purdue.edu (C.H.L.); jong@cau.ac.kr (J.L.)

30 min to hours for the device to move one material from one place to another.

To this end, we demonstrate a soft manipulator that can repeat the holding and unloading of thin and fragile materials within 10 s in response to an electrical signal. We hypothesized that a rapid thermo-responsive, microchanneled hydrogel layered with a micro-electric heater would lift and release materials of interests without applying an external force due to temperature-induced internal pressure change in microchannels of the gel (Fig. 1). In addition, gels tailored to be as soft as biological suction cups would allow fast and notable changes in internal pressure in response to small temperature changes while minimizing the amount of force imparted onto the thin material to be transported. We examined this hypothesis by attaching a flexible electric heater, which converts electrical signals into heat, to a microchanneled PNIPAAm hydrogel. We examined the extent that the electrothermal signal controls the shrinkage and expansion of microchannels of the gel along with subsequent pressure change inside microchannels. The resulting soft manipulator was assessed for its ability to lift up and release thin materials onto target tissues promptly in response to the electrothermal signal. These thin materials include therapeutic stem cell sheets and ultrathin, wearable bioelectronic devices.

RESULTS AND DISCUSSION

We prepared a hydrogel that undergoes a rapid volumetric change in response to a temperature change by introducing anisotropically aligned microchannels into the PNIPAAm gel. The microchanneled gel was assembled by placing the pregelled NIPAAm solution on top of a liquid nitrogen reservoir. Then, ice crystals nucleated from the bottom and grew to the top surface due to the temperature gradient (step 1 in Fig. 2A). Simultaneously, solutes, including NIPAAm monomer, cross-linker, and photo-initiator in the solution, were separated from the growing ice crystals because of the decreased solubility in ice crystals (step 2 in Fig. 2A). This continuous and directional segregation of the solutes formed a cryo-concentrated phase between growing ice crystals. Subsequent exposure of the frozen sample to ultraviolet (UV) light–activated polymerization and cross-linking reaction fixed the anisotropically aligned PNIPAAm network (step 3 in Fig. 2A) (*18*, *19*). The final washing process with the water removed ice crystals and created a PNIPAAm gel with continuously aligned microchannels (Fig. 2B). The resulting gel exhibited an average microchannel diameter of ~20 ± 4 μm and an average wall thickness of 0.2 μm in the gel at room temperature (Fig. 2C). The porosity reached 95 ± 1%.

For comparison, randomly oriented water crystals were created in the PNIPAAm gel by placing the pregelled NIPAAm solution in a freezer at −25°C and curing it under UV light. The resulting hydrogel showed a similar porosity to the PNIPAAm gel prepared by directional crystallization. However, the microchannels of varying diameters were oriented randomly (fig. S1). In addition, PNIPAAm gel free of microchannels was prepared by skipping the crystallization step.

We examined the equilibrium swelling ratios (ESRs) of the resulting gels. All samples showed the volumetric swelling change at around 32°C, which corresponds to the lower critical solution temperature (LCST) of PNIPAAm (Fig. 2D). The difference in the ESR between 25° and 35°C was dependent on the microchannel architecture of the gel. In particular, gels with anisotropically aligned microchannels showed a 2.7-fold higher swelling ratio than those with randomly oriented microchannels and a 1.4-fold higher swelling ratio than those free of microchannels. The elastic modulus of the gel with anisotropically aligned microchannels was dependent on the direction of microchannels (Fig. 2E). The elastic modulus measured by compressing the gel perpendicular to the microchannel was 2.4 kPa, which was twofold lower than that measured by compressing the gel in parallel with the microchannels. In contrast, the gel with randomly oriented microchannels and the gel free of microchannels showed the minimal dependency of the elastic modulus on the direction of compression.

Next, we examined the extent that the microchannel architecture of the gel modulates the volumetric swelling rate in response to temperature change. The gel without microchannels exhibited minimal volumetric change over 10 s when the temperature was increased from 25° to 40°C. In contrast, the gel with anisotropically aligned microchannels reduced its volume by 60% within 10 s when

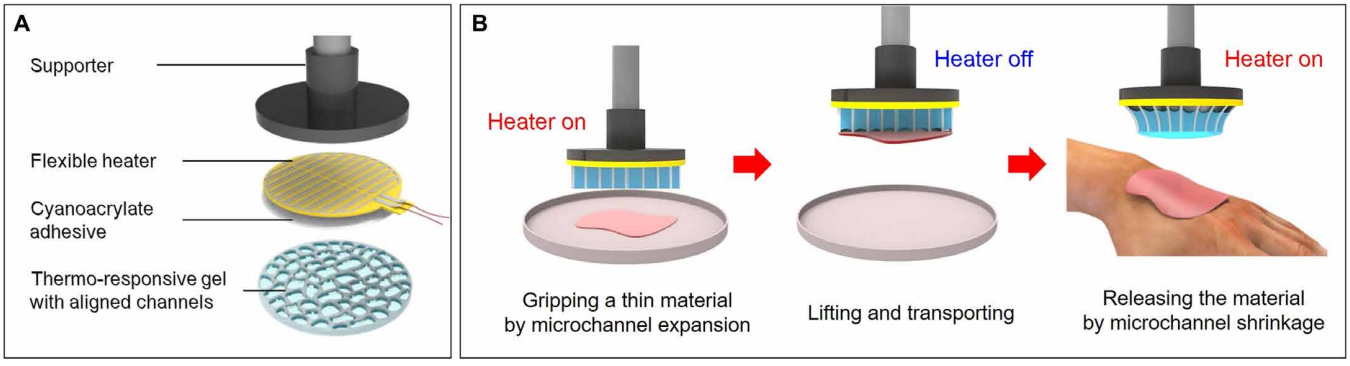

Fig. 1. Design of the electrothermal soft manipulator for delicate material transport. Schematic illustration of (**A**) the soft, electrothermally controlled manipulator and (**B**) the process to transport a thin material using the soft manipulator. (A) The soft manipulator consists of a supporter, flexible heater that can convert electrical current to heat, cyanoacrylate-based wet adhesive, and a thermo-responsive PNIPAAm hydrogel with aligned microchannels. (B) Process to transport materials of interests using the soft manipulator. First, the soft manipulator is lowered to let the gel contact a thin material such as a therapeutic cell sheet or an ultrathin film device. During this step, the heater is turned on to contract microchannels of the gel. Second, the heater is turned off to open microchannels of the gel and generate negative pressure in microchannels. As a consequence, the gel serves to hold, lift up, and transport the thin material. Third, the heater is turned on to close microchannels of the gel and, in turn, generate positive pressure in the microchannels. The positive pressure serves to release the thin material onto the target surface.

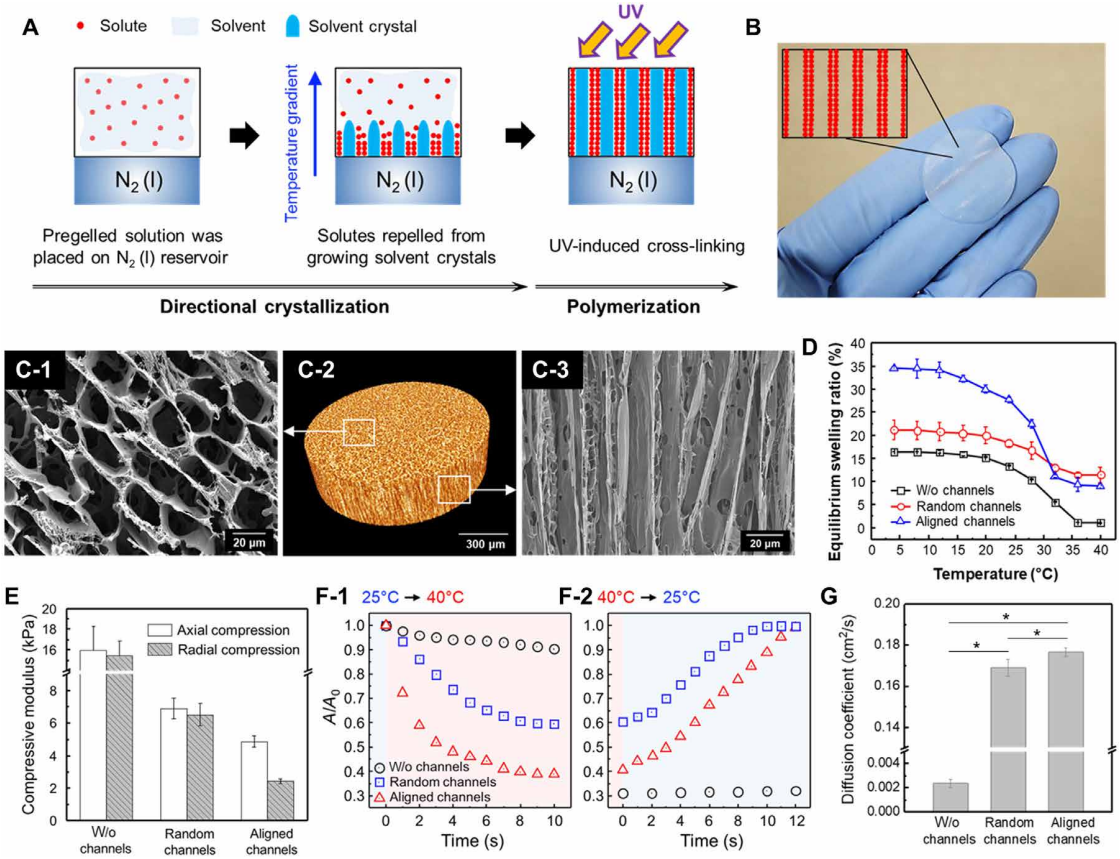

Fig. 2. Fabrication and analysis of rapid temperature-responsive gel. (**A**) Schematic illustrating the fabrication process of the gel with anisotropically aligned microchannels. The gel is prepared by directional crystallization and subsequent polymerization. (**B**) Photograph of the resulting microchanneled hydrogel after swelling in water. (**C**) Microstructure of the gel: (C-1) scanning electron microscopy (SEM) micrograph of the top surface, (C-2) 3D imaging of the microchanneled hydrogel via micro–computed tomography (micro-CT), and (C-3) SEM micrograph of microchannels that connect the top and bottom of the gel. (**D**) ESR of gels at different temperatures. (**E**) Compressive elastic moduli of gels. Samples were compressed in parallel with microchannel direction (axial compression) and perpendicular to microchannel direction (radial compression). (**F**) Time-dependent volumetric changes of microchanneled gel on heating (F-1) and cooling (F-2). The samples were placed on 40° or 25°C plate. The resulting volumetric change was recorded. (**G**) Effective diffusion coefficient of water in gels quantified by the reswelling plot (F-2). * represents the statistical significance of the difference of values between conditions indicated with line (*$P < 0.01$). Photo credit: Byoungsoo Kim, University of Illinois at Urbana-Champaign.

temperature increased to 40°C (Fig. 2F-1 and movie S1). This heat-triggered shrinkage is attributed to the decrease of the average cross-sectional diameter of microchannels from 20 to 9 μm as examined with scanning electron microscope images (fig. S2). The microchannel alignment was maintained during the shrinkage. The gel with randomly oriented microchannels also shrank within 10 s when temperature increased to 40°C (Fig. 2F-1). However, the degree of shrinkage was approximately 0.4, which was 20% lower than the gel with anisotropically aligned microchannels. The electron microscopic images showed lots of open voids as well as micropores collapsed incompletely (fig. S3). In contrast, the gel with aligned microchannels exhibited a more uniform decrease in the microchannel diameter and minimal macro-sized voids after heating (fig. S2). This result indicates that micropores of varying diameters and orientation limit heat-induced collapse, thus leading to the decreased volume shrinkage.

Cooling the gel from 40° to 25°C resulted in gel expansion. The speed and degree of volumetric expansion were dependent on the microchannel architecture. The gel without microchannels did not recover its original volume even after 1 hour (Fig. 2F-2 and fig. S4). In contrast, both of the gels with microchannels restored their original volume within 10 s due to reswelling. The reswelling plot displayed in Fig. 2F-2 was used to quantify the effective water diffusion coefficient (Fig. 2G). We used the Higuchi equation derived under the steady-state approximation of Fick's law of diffusion as follows (*20*)

$$V_t = V_{25} \cdot (S/V_{40}) \cdot (D' \cdot t/\pi)^{1/2} \quad (1)$$

where V_t is the volume of a gel at time t, D' is an effective diffusion coefficient, and S is an effective surface area. V_{40} and V_{25} are the volume of a gel at 40°C and 25°C, respectively. We assumed that water diffusion occurred exclusively on the gel surface. Anisotropically microchanneled gels had a 75-fold higher water diffusion rate than the gel free of microchannels (Fig. 2G). In addition, the gel with anisotropically aligned microchannels showed a 10% higher water diffusion rate than that of the gel with randomly oriented microchannels.

Separately, a flexible electric (joule) heater was fabricated to be attached to the gel by photolithographic patterning of a copper/polyimide film (thickness, 9-μm copper/12-μm polyimide). The

linewidth and spacing of the copper pattern was kept at 300 μm to provide uniform heat across the gel disk (Fig. 3A). The heater was additionally coated with a layer of tin (thickness, ~1 μm) to prevent oxidation of the copper at an increased temperature within a humid environment. The heater was then connected to an external power supply with a voltage range of 2 to 5 V (Fig. 3B). The activated temperature was examined using an infrared camera, showing that the heater reached the target temperature at 37°C within 5 s after applying a voltage of 2 V (Fig. 3, A and B). After the power was turned off, the temperature was dropped immediately back to 25°C. Such electrothermal heater was attached to the gel disk using a cyanoacrylate-based adhesive (*21*). The bilayered hydrogel-heater construct was finally attached to a three-dimensional (3D) printed supporter (Fig. 3C).

With the resulting electrothermal soft manipulator, we examined the response of the gel disk to the electrical signal. The test was conducted outside water. Figure 3 (D and E) shows the side view of the gel disk and the microstructural changes of the gel surface during the electrically controlled heating and cooling cycle. Switching on the heater triggered shrinkage of microchannels within 10 to 20 s and simultaneously released a fraction of water from the gel (Fig. 3D and movie S2). With the power off, the gel expanded the microchannels and reabsorbed the water within a few seconds (Fig. 3E and movie S2). The shrinkage and expansion of microchannels could be repeated hundreds of times by turning the power on and off. No structural failure of the gel was observed during repeated operation. We further examined the heat transfer through the gel layer placed on the heater at a temperature of 40°C (fig. S5A and movie S3). With the heater on, the temperature of the gel increased rapidly from the bottom (point 1 in fig. S5B) to a top (point 4 in fig. S5B) within 20 s. This result confirms heat propagation along the gel thickness direction. The gel temperature increased at a rate of 0.3°C/mm·s, independent of the region of observation. Last, the temperature of the entire gel became equal to that of the heater within 30 s (fig. S5C).

The gel with randomly oriented microchannels also underwent shrinkage and expansion in response to the electrothermal signal. However, the area undergoing microchannel shrinkage and expansion was not as uniform as in the gel with anisotropically aligned microchannels (fig. S6). Therefore, the gel released water locally. The gel without microchannels showed a very slow release and limited absorption of water when the electric heater was on and off, respectively (fig. S7).

The shrinkage and expansion of anisotropically aligned microchannels allowed the gel to grip, lift, and release materials of interest (Fig. 4A and movies S4 and S5). The manipulator with a diameter of 25 mm was used in this study. The manipulation process was conducted as follows. First, we shrank the upper part of the microchannels of the hydrogel by activating the heater (stage 1 in Fig. 4A). During this process, the gel released a fraction of water, thus creating an empty pocket between the heater and residual water in the microchannels. The gel was then placed on a 4-inch-diameter silicon wafer, a model material that should be transported (stage 2 in Fig. 4A). Next, the heater was deactivated to expand the shrunken microchannels and move residual water upward [stage 3 (i) in Fig. 4A]. The subsequently formed vacant space between water within the microchannels and the silicon wafer decreased the pressure inside microchannels,

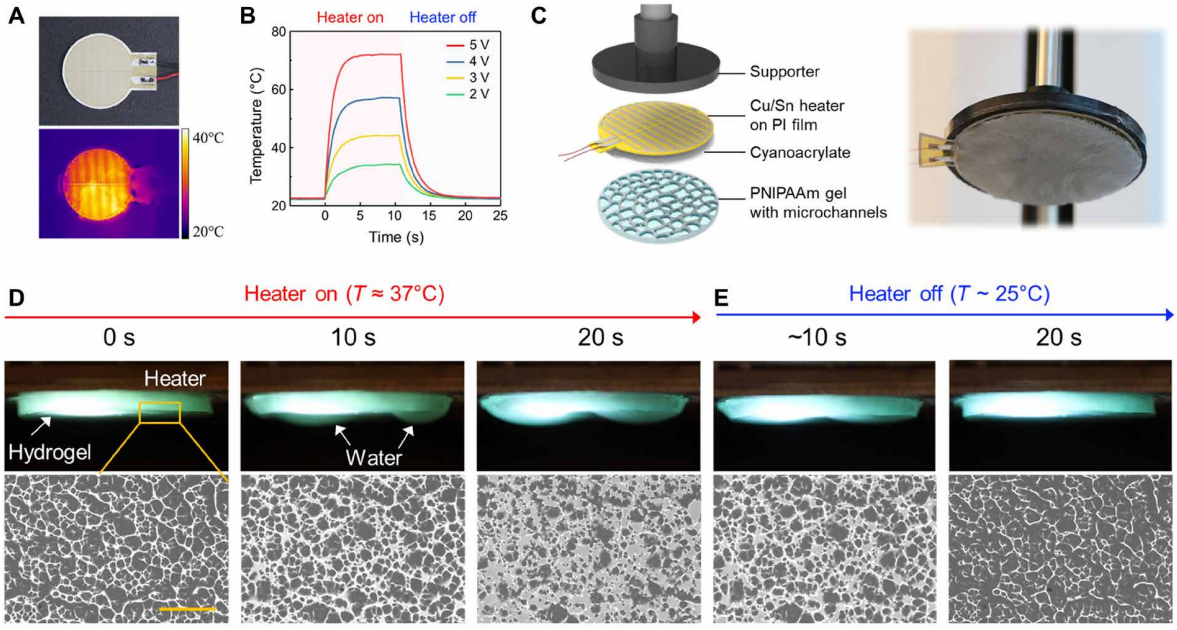

Fig. 3. Design of soft, electrothermal soft manipulator. (**A**) Photograph (top) and a thermal image of the flexible heater captured using an infrared camera (bottom). (**B**) Temperature change over time at differently applied voltages. The temperature profiles of the heater were obtained using an infrared camera. (**C**) Structural configuration of the soft manipulator (left) and a photograph of the soft manipulator (right). (**D** and **E**) Top: Snapshots of the microchanneled gel in the soft manipulator when the heater was turned on (D) and off (E). Images on the second row represent optical microscopic images of the gel surface when the heater was turned on and off. When the heater was turned on, aligned microchannels of the gel pushed water out while being closed for 20 s (D). When the heater was switched off, the gel in the soft manipulator opened microchannels and pulled water back into microchannels within 20 s (E). Scale bar, 100 μm. Photo credit: Byoungsoo Kim, University of Illinois at Urbana-Champaign.

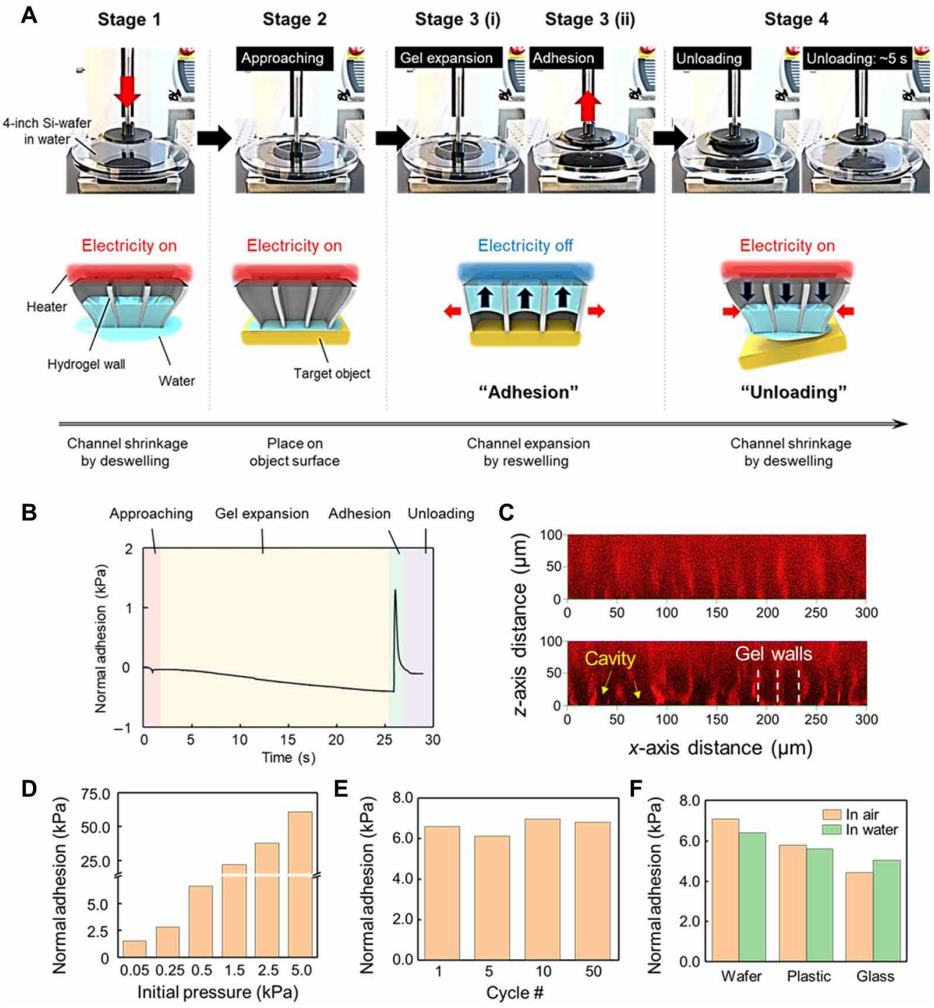

Fig. 4. Working mechanism and characterization of the soft manipulator. (**A**) Snapshots showing the transport of a 4-inch-diameter silicon wafer using a soft manipulator (upper images). Schematic illustrating the shrinkage and expansion of microchannels and subsequent water movement in microchannels controlled by the electrothermal signal (bottom images). The operating power of the soft manipulator was 5 W. (**B**) The time-dependent variation of normal adhesion strength measured by the dynamic mechanical analyzer (DMA) during stages 2 and 3 in (A). An initial contact strength of 0.05 kPa was applied to the soft manipulator for this measurement. (**C**) Fluorescence images of water in microchannels of the gel. The image was obtained from a 3D *z*-stack confocal microscope before (top) and after adhesion (bottom) of the soft manipulator to a target surface. The heater was attached to the upper part of the gel. (**D**) Dependency of the adhesion strengths on the initial load. (**E**) Variation in the adhesion strength as a function of cycle number. (**F**) Adhesion strength of the soft manipulator measured with the various target substrates in water and air. An initial contact strength of 0.5 kPa was applied to the soft manipulator using DMA for this measurement. Photo credit: Byoungsoo Kim, University of Illinois at Urbana-Champaign.

thus making the gel adhere to the silicon substrate. Thus, the soft manipulator could lift the substrate [stage 3 (ii) in Fig. 4A]. Last, with the power on, microchannels adjacent to the heater shrank and pushed water out of the microchannel (stage 4 of Fig. 4A). The subsequent pressure increases inside the microchannels served to dislodge the silicon wafer quickly. This mechanism is distinct from artificial handling systems assembled with an inspiration from anatomy of the cephalopods suction cup. These handling systems, however, require external force to hold and release materials of interest. In contrast, the manipulation process performed by our soft manipulator resembles the neuromuscular actuation in which cephalopods grip and release materials of interests. Through control of electricity, the rapid electrothermal actuation of the gel enabled the manipulator to systematically lift up and release target materials without external forces.

The normal pressure development of the gel to the silicon surface was further measured, particularly during stages 2 and 3. This measurement was conducted by attaching the bilayered gel-heater construct to a dynamic mechanical analyzer (DMA) (Fig. 4B). First, the gel was preheated by the heater and brought into contact with a 4-inch silicon wafer ("Approaching" stage in Fig. 4B). Next, when the power was turned off to expand microchannels, the load was increased in the negative direction for 25 s ("Gel expansion" stage in Fig. 4B). This bilayered gel-heater construct was then slowly pulled upward at 0.1 mm/s by DMA to monitor the increase of the adhesion strength ("Adhesion" stage in Fig. 4B). The maximum adhesion

strength reached 1.5 kPa. Once the power was turned on before the stress reached 1.5 kPa, the normal adhesion strength decreased quickly to 0 kPa within 5 s ("Unloading" stage in Fig. 4B).

Without temperature control, the manipulator does not exhibit adhesion. We further examined whether temperature-induced contraction and expansion of microchannels are essential to create adhesion. The soft manipulator preheated to 37°C was placed on the silicon wafer immersed in water with controlled temperatures. Then, the heater of the soft manipulator was turned off. At temperatures below LCST of the gel layer (i.e., ~32°C), the adhesion strength increased rapidly with decreasing temperatures (fig. S8). This result confirms that temperature of the heating layer in the manipulator controls the degree of expansion of the microchanneled gel layer and, in turn, regulates adhesion strength.

We propose that the electrothermally controlled adhesion of the gel to the silicon wafer results from the pressure difference (ΔP) between two ends of microchannels. We introduced the mixture of rhodamine B and water into microchannels of the gel and monitored the vertical movement of water through the individual microchannel during stage 3 (i) in Fig. 4A. According to the side view of the gel captured with confocal microscopy, the microchanneled gel disk was fully filled with water (Fig. 4C, top). Heating and the subsequent cooling process resulted in the space in the lower part of the microchannel adjacent to the silicon substrate by moving residual water upward in the microchannels (Fig. 4C, bottom). This image is similar to the scheme that represents stage 3 in Fig. 4A. The average height of space in the microchannel was approximately 50 μm. The pressure difference of a single microchannel in the gel was quantified with a height of the empty part in the microchannel as follows

$$\Delta P = \rho_w \cdot g \cdot (h_i - h_f) \quad (2)$$

where ρ_w is the density of water, g is the gravitational acceleration, and h_i and h_f are the height of the space in microchannels when the power was turned on and off, respectively. According to the calculation, each microchannel in the gel produced 0.5 Pa of negative pressure after the cooling process.

The adhesion strength of the gel to the silicon wafer was dependent on the initial load applied to the soft manipulator (Fig. 4D). The maximum adhesion strength reached 65 kPa with the initial pressure of 5.0 kPa. The maximum adhesion strength reached 65 kPa with the initial pressure of 5.0 kPa. To underlie the mechanism, we examined the normal pressure development that varies with the initial contact pressure using a DMA. As shown in fig. S9A, the heated soft manipulator was placed on the target silicon wafer. As soon as the heater was turned off, the gel layer expanded and pushed the silicon wafer more strongly. As a consequence, the normal pressure developed in the opposite direction. The normal pressure increased with the initial contact pressure (fig. S9B). Increasing the initial contact pressure enlarged the effective suction area of the soft manipulator and also augmented the normal pressure.

We also examined the effect of elastic modulus of target materials on the adhesion strength. We prepared alginate hydrogels with elastic moduli of 22.5 and 69.8 kPa as target materials for transport (fig. S10A). As confirmed with the pressure development profiles, with a given initial contact pressure of 0.25 kPa, the soft manipulator exhibited a similar magnitude of the adhesion strength to the alginate gels as well as the silicon wafer with a much higher elastic modulus of 140 to 180 GPa. This result suggests that it is not necessary to vary the initial contact pressure with the target material stiffness (fig. S10B). The adhesion strength was not reduced during the repeated cycles of closure and opening of microchannels (Fig. 4E). No chemical contamination or residue was observed on the silicon wafer after the process (fig. S11). The soft manipulator could transport plastic and glass materials by exerting a similar magnitude of the adhesion strength regardless of material hydrophobicity (Fig. 4F). The soft manipulator functioned to transport materials immersed in aqueous media and those in the air.

Last, we examined the capability of the soft manipulator to lift up, transport, and release ultrathin and delicate materials, such as living cell sheets and ultrathin thin film devices. We prepared a single-layered mouse skeletal myoblast cell sheet on a culture dish. In general, monolayered cell sheets were easily damaged or crumpled when picking up the sheet from the cell culture dish with forceps (Fig. 5A and movie S6). By switching the heater of the soft manipulator on and off, it was possible to lift the myoblast cell sheet and transport them to the new target sites. First, we transferred the cell sheet to a glass dish using the soft manipulator (Fig. 5B). Then, we examined whether the soft manipulator damages the sheet during transplantation. Off-axis deformation and viability of the cell sheet before and after delivering process were measured using the spatial light interference microscopy (SLIM) and the live-dead assay kit, respectively. According to SLIM observation and live-dead assay results, there was no substantial wrinkling nor loss of viability of cells that formed the cell sheet during this transport process (Fig. 5C and fig. S12). This simple transportation process allowed us to fabricate a 3D tissue by stacking multiple myoblast sheets using the soft manipulator (Fig. 5D). The resulting three-layered myoblast tissue showed a dense construct with three different layers.

The soft manipulator allowed us to pick up various types of cell sheets and deliver them rapidly to any target surfaces. As a demonstration, we delivered the myoblast cell sheet to an ex vivo muscle tissue without any structural breakages (Fig. 5E and movie S7). The entire transport process could be completed within 30 s. In contrast, the soft manipulator assembled using a gel with randomly oriented micropores could not uniformly deliver the cell sheet due to the nonuniform micropore shrinkage (fig. S13). We also used the soft manipulator as a device to support atraumatic transplantation of a stem cell sheet to the anterior surface of the cornea. Similar to the myoblast cell sheet, mesenchymal stem cell sheets on a donor substrate could be easily transferred to the corneal epithelium of a rat eye (Fig. 5F). We confirmed the stable attachment of the stem cell sheet to the anterior surface of the cornea, in the position of the corneal epithelium of the rat eye by histological observation (Fig. 5G). A method to atraumatically transplant ex vivo generated stem cell sheets could simplify surgical technique and expand access to corneal epithelial stem cell transplants and it could have useful application in the treatment of corneal epithelial injuries, persistent epithelial defects, limbal stem cell deficiencies, nonhealing corneal ulcers, and blast injuries (*22*, *23*).

In addition, the soft manipulator was used to transport an ultrathin electrophysiological (EP) sensor (thickness, ~1 μm) without causing wrinkling. We fabricated the EP sensor that consists of reference, ground, and measurement electrodes allowing high-quality recording of electrocardiogram (ECG) signals (Fig. 6A) (*24*, *25*). Generally, such ultrathin film devices were easily crumpled when picking up from a donor substrate, which typically requires the use

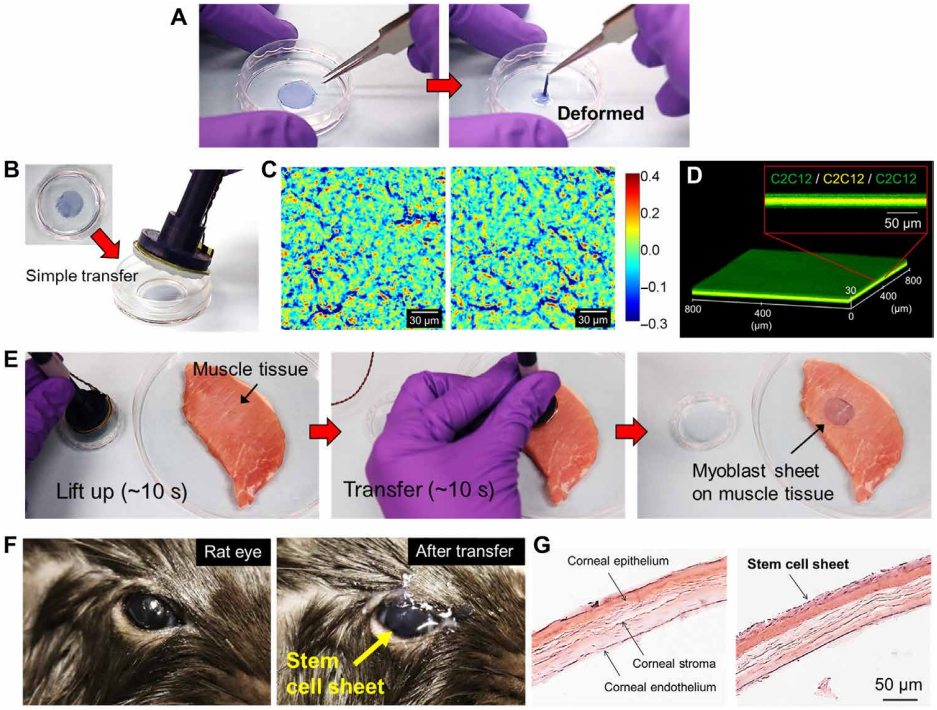

Fig. 5. Demonstration of the ability of the soft manipulator to transport cell sheets to target sites. (**A**) Snapshots of a process to pick up a skeletal myoblast sheet with forceps. The cell sheet was deformed when picking up the sheet using forceps (right). The cell sheet was stained with methylene blue for visualization. (**B**) Snapshot of a process to transport the skeletal myoblast sheet onto a glass surface using the soft manipulator. (**C**) Spatial light interference microscopy (SLIM) images of the cell sheet before (left) and after (right) the transfer, showing off-axis diffraction of the cell sheet. (**D**) Fluorescence image of a multilayered cell sheet consisting of three different myoblast sheets. The multilayered sheet was prepared by stacking cell sheets using the soft manipulator. (**E**) Snapshots of a process to transport a skeletal myoblast sheet onto a muscle tissue. It took 30 s for the entire transfer process. (**F**) Photographs of a rat eye before and after transplantation of a stem cell sheet. The cell sheet transplanted to the corneal epithelium of a rat eye using the soft manipulator. It took 30 s for the entire transfer process. (**G**) Histological examination of the rat eye before (left) and after (right) a stem cell sheet transfer. Hematoxylin and eosin staining revealed that the stem cell sheet was able to be successfully transplanted onto the anterior corneal surface without substantial interface space generation. Photo credit: Byoungsoo Kim, University of Illinois at Urbana-Champaign.

of a temporary handling support (fig. S14 and movie S8). By using the soft manipulator, it was possible to controllably transfer the EP sensor from the donor substrate to the surface of the pig heart within a minute (Fig. 6B and movie S9). No substantial wrinkles were observed after completing the transport (Fig. 6C). A waveform generator was used to apply a preprogrammed ECG signals across the pig heart using an Ag/AgCl electrode. The resulting ECG signals captured from the EP sensor were nearly identical to those generated from the waveform generator (Fig. 6D and fig. S15). The Pearson's correlation coefficient of the signals was 0.98.

Together, this study demonstrates that the soft manipulator assembled by integrating a rapid thermal-responsive microchanneled gel and an electrothermal heater can transport ultrathin biological and electronic materials quickly and safely. The resulting soft manipulator could be switched on and off with electricity to lift and release thin and delicate materials within tens of seconds. This rapid handling could be attained with the electrothermally controlled change in the adhesion force between the soft manipulator and target materials. Such an actuation mechanism is very similar to the muscular action of cephalopod suction cups. Therefore, this soft manipulator is distinct from previous suction cup–mimicking platforms that need external force for detachment of materials. In addition, the soft manipulator could move thin materials of interest in both wet and dry conditions. Using this unique functionality, we could assemble multilayered cell sheets and place an ultrathin biosensor to the target tissue without impairing its function.

We envisage that further modification of this soft manipulator with an electronic sensor would allow robots to transport ultrathin materials autonomously. For instance, the resulting smart soft manipulator would be able to monitor the degree of deformation of transporting materials during contact and, in turn, adjust the suction force to a level at which materials retain their structural integrity and functionality. By doing so, the soft manipulator would improve its performance from the standpoint of safety and accuracy of material handling and assembly. We believe that the present design concept may be widely used as a new soft handling tool for the fabrication of ultrathin film devices, tissue engineering, and transplant surgery.

This study demonstrated an electrically controllable soft machinery useful to transport ultrathin, delicate objects, including therapeutic cell sheets and thin, wearable biosensing devices. This system, named as the electrothermal soft manipulator, consisted of a flexible heater attached with a rapid thermo-responsive PNIPAAm hydrogel disk with controlled microchannel architecture and tissue-like softness. Compared with hydrogels free of microchannels or those with randomly oriented microchannels, the anisotropically aligned PNIPAAm hydrogel could shrink and expand in response to

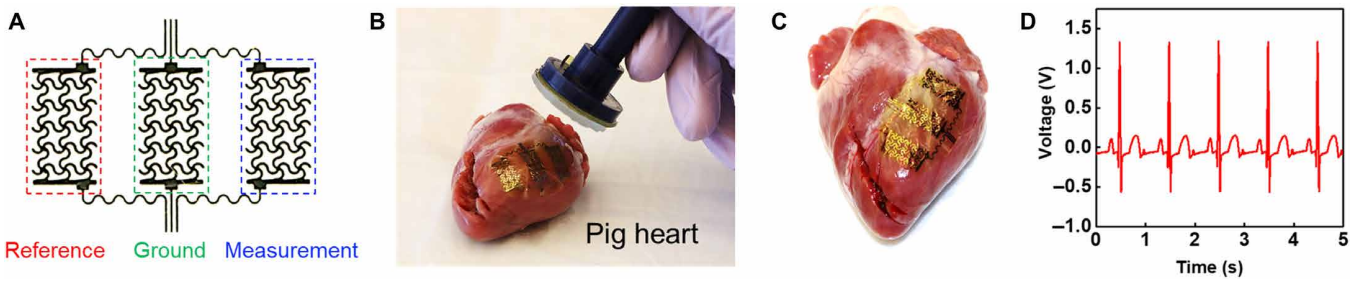

Fig. 6. Transportation of an ultrathin EP sensor. (**A**) Device configuration of the ultrathin EP sensor (t = 1 μm) tailored for the measurement of ECG signals. (**B**) Snapshot of a process to transport the device to the surface of the pig heart. It took 30 s to capture and deliver the device onto the pig heart. (**C**) Photograph of the device transplanted to the pig heart using the soft manipulator. (**D**) Representative ECG signals measured using the transplanted device. Photo credit: Byoungsoo Kim, University of Illinois at Urbana-Champaign.

the electrically induced heat much faster, on the order of seconds. Such a fast-volumetric change of the microchannels on the surface of an object could produce and remove pressure-induced adhesion repeatedly. This controlled actuation mechanism is similar to the activity of cephalopod suction cups that hold and release objects of interest using bioelectric signals. As a consequence, the soft manipulator could move thin biological and bioelectronic devices quickly in both wet and dry conditions without causing wrinkling or damage of the thin materials. Such an electrothermally controlled soft manipulator would be useful to various applications that require the sophisticated manipulation of fragile and delicate biological tissues and bioelectronic devices.

MATERIALS AND METHODS

Preparation of the microchanneled PNIPAAm gel

NIPAAm (1.25 g) and *N*,*N*′-methylenebisacrylamide {12.5 mg [0.01 weight % (wt %) of NIPAAm]} were dissolved in distilled water (8.75 ml) for 1 day at 25°C to ensure the complete dissolution. Then, 25 mg (0.5 wt % of NIPAAm) of radical photo-initiator (Irgacure 2959) was added into the obtained solution and stirred until all the solids completely dissolved. The resulting pregelled NIPAAm solution was poured onto a Si-wafer substrate (4 inches, 550 μm thick) with silicone mold (50 mm by 50 mm by 1 mm or 20 mm by 20 mm by 10 mm). Then, the Si-wafer substrate was put on a liquid nitrogen reservoir for the directional crystallization of the pregelled NIPAAm solution. The distance between the bottom surface of the Si-wafer and the top surface of liquid nitrogen was 1 cm. After complete crystallization of the pregelled NIPAAm solution, the samples were irradiated with a UV lamp (λ = 365 nm) for 6 hours at a −25°C freezer for the radical cryo-polymerization. The as-prepared poly-NIPAAm gel (PNIPAAm) was then washed with fresh water three times to remove the ice crystals.

For comparison, PNIPAAm gel with randomly oriented microchannels was prepared by placing the pregelled NIPAAm solution in a freezer at −25°C for random crystallization. Then, the resultant samples were cryo-polymerized and washed at the same condition described above. PNIPAAm gel free of microchannels was prepared by skipping the crystallization and subsequently irradiated with a UV lamp for 1 hour at 4°C. All hydrogel samples were soaked in 250-ml distilled water at 25°C, which was repeatedly replaced for 1 day to remove unreacted impurities before using them.

Characterization of PNIPAAm gels

The morphology of microchanneled PNIPAAm gels was examined using an environmental scanning electron microscope (ESEM; Quanta FEG 450, FEI) and microcomputed tomography (micro-CT, MicroXCT-200, Xradia Inc.). For cross-sectional analysis, the samples were immersed in liquid nitrogen for 30 min and immediately cryo-fractured. One hundred points from 10 different ESEM images were taken to determine the average pore size. The porosity of gels was determined by the gravimetric method. The pore volume of gels was divided by the total volume of gels as follows

$$\text{Porosity}(\%) = \{(W_{\text{swollen}} - W_{\text{dry}})/\rho_{\text{w}}\}/\{(W_{\text{swollen}} - W_{\text{dry}})/\rho_{\text{w}} + (W_{\text{dry}}/\rho_{\text{PNIPAAm}})\} \quad (3)$$

where W_{swollen} and W_{dry} are the weights of swollen and dry gels, respectively; ρ_{w} is the water density; and ρ_{PNIPAAm} is the NIPAAm density (1.1 g/cm^3).

For ESR measurement, we measured the weight of PNIPAAm gels at different temperatures (4° to 40°C) with 4°C increments. The ESR was defined using the following equation

$$\text{ESR}(\%) = \{(W_{\text{s}} - W_{\text{d}})/W_{\text{d}}\} \cdot 100 \quad (4)$$

The hydrogel samples were equilibrated at each temperature for 12 hours and weighted (W_{s}) after removing excess water. The dry weight of the samples (W_{d}) was measured after lyophilization. Five samples of each PNIPAAm gel were averaged.

For dynamic deformation analysis of hydrogels in response to temperature change, hydrogel samples immersed in 25°C were trimmed into a cylinder shape (d = 25 mm, t = 1 mm) and placed on a copper plate (t = 1 mm). Then, the plate was put onto a heated Peltier stage (40°C) to investigate the deswelling kinetics of samples. For reswelling kinetics, deswelled samples were transferred to a cooled Peltier stage (25°C). We monitored the volume change in response to temperature using an optical microscope that connected with the Peltier device (TP104SC-mK2000A, Instec). All optical images were analyzed using ImageJ software.

The compressive modulus of hydrogels was measured on an electronic universal testing machine (Instron 5943, Instron) equipped with a water bath. Samples were cut into a square shape (10 mm by 10 mm by 10 mm). All mechanical tests were conducted in a water bath (25°C). There were five replicates for all mechanical tests.

Preparation of the flexible (joule) heater

The heater was fabricated on a copper/polyimide film (t = 9 μm/12 μm, Pyralux AC091200EV, Dupont). A standard photolithographic patterning with a dry film photoresist (Riston MM540, Dupont) followed by the wet etching method (CE-100, Transene Inc.) defined the copper layer into a joule heating element. The copper traces were coated with 1-μm layer of tin (Sn) (421 Liquid Tin, MG Chemicals) to protect the copper from oxidation in elevated temperatures within a humid environment. The resulting heater was then connected to an external power supply, where a voltage range of 2 to 5 V and its thermal characterizations over time were recorded using an infrared camera (E40, FLIR Systems).

Fabrication of the soft manipulator

The cyanoacrylate-based adhesive was spread on top of the flexible heating array (*21*). Immediately after, the hydrogel was trimmed into a cylinder shape (d = 25 mm, t = 1 mm) and pressed onto the substrate. The bonding occurs within 30 s. The resulting gel/heater was attached to a 3D printed supporter using double-sided tape (VHB, 3M). Then, the soft manipulator was connected to an electrical power supply.

Characterization of the soft manipulator

For dynamic deformation analysis of the soft manipulator in response to activation of a heater, a monochrome camera (DS-Qi2, Nikon) was attached to an optical microscope (Eclipse LV100, Nikon) for top-view analysis of the gel in the soft manipulator. A digital camera with an optical zoom macro lens (Canon, MP-E 65 mm) was used for the side view analysis of the soft manipulator. Gels in the soft manipulator were incubated with colored water (Green, McCormick) for visualization of water.

Adhesion tests were performed with a DMA (ESM303, Mark-10). The soft manipulator was mounted on a load cell of the DMA (M5-5 or M5-200, Mark-10), and the vertical approach and retraction speeds of the soft manipulator were 0.1 mm/s. Force-displacement profiles with time were measured at room temperature.

To examine the capability of the soft manipulator to handling materials with different elastic moduli, alginate hydrogels with elastic moduli of 23 and 70 kPa were used in this study. Pregelled alginate solution was prepared by mixing 2 wt % alginate solution in MES buffer (pH 6.5) with sulfonated *N*-hydroxysuccinimide and 1-ethyl-3-(3-dimethylaminopropyl) carbodiimide. Then, the pregelled alginate solution was cross-linked by adding adipic acid dihydrazide (AAD). The elastic modulus of the alginate gels was controlled by varying the molar ratio between AAD and uronic acids of alginate (M_{AAD}).

Cross-sectional fluorescence images were obtained from 3D z-stack confocal images (LSM 880, Carl Zeiss). We used Rhodamine B mixed with water for tracking of water inside the soft manipulator before and after the attachment process.

To investigate surface contamination of the soft manipulator, we performed adhesion tests to silicon wafers using either the soft manipulator or a commercial medical grade tape (Transpore, 3M). After detachment of the samples, the resulting wafer was incubated with a dye (Rhodamine B) for 30 min. All samples were washed with distilled water three times in total. Then, we dried the wafer surface using N_2 gas and subsequently observed the wafer surfaces using fluorescent optical microscopy.

Preparation of stem cell sheets

C2C12 cells (mouse skeletal myoblast cell line, CRL1772) and D1 cells (bone marrow–derived mesenchymal stem cell line, CRL12424) were obtained from the American Type Culture Collection (ATCC). C2C12 or D1 cells were plated on temperature-responsive PNIPAAm-grafted culture dishes (d = 35 mm, UpCell, Thermo Fisher Scientific) with seeding density of 5×10^5 cells. The cells were then cultivated for 3 days according to the guidelines of ATCC. To harvest sheets, confluent cells were rinsed twice with warmed Dulbecco's phosphate-buffered saline (DPBS). Then, the monolayers were detached from the culture dish by lowering the incubation temperature from 37° to 20°C.

Analysis of cell sheets after transport using the soft manipulator

The viability of cell sheets was examined using the LIVE/DEAD Viability/Cytotoxicity Assay Kit for mammalian cells (Invitrogen) according to the manufacturer's instructions. The cultured cells or transferred cells were gently washed three times with DPBS. Calcein acetoxymethyl (AM) and ethidium homodimer-1 (EthD-1) were diluted together in DPBS. Diluted calcein AM and EthD-1 solution (1 ml) was added to cultured cells and kept for 45 min at room temperature. The live cells were stained with calcein AM, and dead cells were stained with EthD-1. After staining, cells were gently washed with 1× DPBS for three times and imaged with a fluorescence microscope (LSM-880, Carl Zeiss). Off-axis deformation of the cell sheets before and after the delivery process was quantified using SLIM. The optical system was assembled by attaching a SLIM module (CellVista SLIM Pro, Phi Optics) to the output port of an existing inverted phase-contrast microscope (*26*).

Assembly of a multilayered cell sheet using the soft manipulator

C2C12 cells were cultured onto a temperature-responsive culture dish to produce cell sheets as described above. After incubation, confluent cells were stained with Cell Tracker Orange CMRA (Invitrogen) or calcein AM (Invitrogen). Then, cell sheets were detached from the culture dish by lowering the incubation temperature from 37° to 20°C. The detached cell sheets were captured and transferred using the soft manipulator with electrical heater control. A multilayered cell sheet was fabricated by repeating the transfer procedure. The resulting multilayered tissue structure was imaged using a fluorescence microscope (LSM-880, Carl Zeiss).

Transplantation of a stem cell sheet onto the anterior surface of the cornea using the soft manipulator

Long-Evans/BluGill rats were used in this study. All experimental protocols were in compliance with the National Institutes of Health Public Health Service Policy on Humane Care and Use of Laboratory Animals and were approved by the University of Illinois at Urbana-Champaign (UIUC) Institutional Animal Care and Use Committee. For fixation of the cornea, the perfusion needle was inserted into the left ventricle of the heart. A cut was made within the right atrium to allow blood evacuation. Saline was injected at a rate of 300 ml/min to clear the blood from the rat, followed by injection of paraformaldehyde (PFA) at 300 ml/min. The perfusion was confirmed by checking PFA dripping from the nose of the rate, stiffening of the extremities and the liver, and contractures of the musculature. After completing the perfusion, the stem cell sheet was placed on the rat's cornea using the soft manipulator. The other

rat eye was used as a control. Enucleation was then performed using microscissors.

Immunohistochemistry and imaging of the stem cell sheet transplanted on the cornea

Enucleation was followed by placement of the eyeball on dry ice then into a mold. The mold was subsequently filled with an optimal cutting temperature (OCT) compound–embedding medium to ensure OCT. Cryosectioning at 40-μm slices was performed using a cryostat. Slices were then fixed using 4% PFA because the eyeball was fixed but not the stem cell sheet. The sample was washed three times in tris-buffered saline (TBS) for 5 min. The section was stained with hematoxylin and eosin staining, followed by dehydration in citrasol for 5 min. The stained tissue section was imaged using Axio Zoom.V16.

Fabrication of the EP sensor and evaluation of its function after placement onto an ex vivo heart using the soft manipulator

The fabrication of the EP sensor began by spin-coating a layer of poly(methyl methacrylate) (PMMA; ~1 μm thick) on a glass substrate, followed by thermal annealing at 180°C for 1 min. A subsequent layer of polyimide (~1 μm thick) was coated and cured in a vacuum oven at 250°C for 1 hour. Thin films of Cr and Au (t = 5 nm/150 nm thick) were deposited by using an electron beam evaporation. Photolithographic patterning using a negative-type photoresist (Riston MM540, DuPont) followed by wet etching with Au and Cr etchants (Transene) defined the joule-heating element. The resulting structure was submerged in acetone to dissolve the bottom PMMA layer. An anisotropic conductive film (ACF; HST-9805-210, Elform) was bonded to the terminals and was connected to an external data acquisition system. The measurement of ECG signals began by attaching two commercial conducting electrodes (30 mm by 24 mm, H124SG, Kendall) diagonally across the pig heart. The electrodes were then connected to an arbitrary waveform generator (3390, Keithley) to apply a preprogrammed cardiac waveform (1-Hz frequency, 50-mV amplitude). The EP sensor was transferred onto the surface of the pig heart with the soft manipulator. The sensor was connected to an external preamplifier (Octal Bio Amp, ADInstruments) and data acquisition unit (PowerLab 16/35, ADInstruments), where the captured ECG signal was digitally filtered with a band-pass filter at the bandwidth of 0.5 to 100 Hz.

SUPPLEMENTARY MATERIALS

Supplementary material for this article is available at http://advances.sciencemag.org/cgi/content/full/6/42/eabc5630/DC1

REFERENCES AND NOTES

1. J. Yang, M. Yamato, C. Kohno, A. Nishimoto, H. Sekine, F. Fukai, T. Okano, Cell sheet engineering: Recreating tissues without biodegradable scaffolds. *Biomaterials* **26**, 6415–6422 (2005).
2. J. Yang, M. Yamato, T. Shimizu, H. Sekine, K. Ohashi, M. Kanzaki, T. Ohki, K. Nishida, T. Okano, Reconstruction of functional tissues with cell sheet engineering. *Biomaterials* **28**, 5033–5043 (2007).
3. K. Nishida, M. Yamato, Y. Hayashida, K. Watanabe, N. Maeda, H. Watanabe, K. Yamamoto, S. Nagai, A. Kikuchi, Y. Tano, T. Okano, Functional bioengineered corneal epithellial sheet grafts from corneal stem cells expanded ex vivo on a temperature-responsive cell culture surface. *Transplantation* **77**, 379–385 (2004).
4. H. Sekine, T. Shimizu, K. Sakaguchi, I. Dobashi, M. Wada, M. Yamato, E. Kobayashi, M. Umezu, T. Okano, *In vitro* fabrication of functional three-dimensional tissues with perfusable blood vessels. *Nat. Commun.* **4**, 1399 (2013).
5. D.-H. Kim, N. Lu, R. Ma, Y.-S. Kim, R.-H. Kim, S. Wang, J. Wu, S. M. Won, H. Tao, A. Islam, K. J. Yu, T.-i. Kim, R. Chowdhury, M. Ying, L. Xu, M. Li, H.-J. Chung, H. Keum, M. M. Cormick, P. Liu, Y.-W. Zhang, F. G. Omenetto, Y. Huang, T. Coleman, J. A. Rogers, Epidermal electronics. *Science* **333**, 838–843 (2011).
6. D.-H. Kim, R. Ghaffari, N. Lu, S. Wang, S. P. Lee, H. Keum, R. D'Angelo, L. Klinker, Y. Su, C. Lu, Y.-S. Kim, A. Ameen, Y. Li, Y. Zhang, B. de Graff, Y.-Y. Hsu, Z. J. Liu, J. Ruskin, L. Xu, C. Lu, F. G. Omenetto, Y. Huang, M. Mansour, M. J. Slepian, J. A. Rogers, Electronic sensor and actuator webs for large-area complex geometry cardiac mapping and therapy. *Proc. Natl. Acad. Sci. U.S.A.* **109**, 19910–19915 (2012).
7. L. Tian, B. Zimmerman, A. Akhtar, K. J. Yu, M. Moore, J. Wu, R. J. Larsen, J. W. Lee, J. Li, Y. Liu, B. Metzger, S. Qu, X. Guo, K. E. Mathewson, J. A. Fan, J. Cornman, M. Fatina, Z. Xie, Y. Ma, J. Zhang, Y. Zhang, F. Dolcos, M. Fabiani, G. Gratton, T. Bretl, L. J. Hargrove, P. V. Braun, Y. Huang, J. A. Rogers, Large-area MRI-compatible epidermal electronic interfaces for prosthetic control and cognitive monitoring. *Nat. Biomed. Eng.* **3**, 194–205 (2019).
8. J.-W. Jeong, W.-H. Yeo, A. Akhtar, J. J. S. Norton, Y.-J. Kwack, S. Li, S.-Y. Jung, Y. Su, W. Lee, J. Xia, H. Cheng, Y. Huang, W.-S. Choi, T. Bretl, J. A. Rogers, Materials and optimized designs for human-machine interfaces via epidermal electronics. *Adv. Mater.* **25**, 6839–6846 (2013).
9. S. De, J. Rosen, A. Dagan, B. Hannaford, P. Swanson, M. Sinanan, Assessment of tissue damage due to mechanical stresses. *Int. J. Rob. Res.* **26**, 1159–1171 (2007).
10. A. Carlson, A. M. Bowen, Y. Huang, R. G. Nuzzo, J. A. Rogers, Transfer printing techniques for materials assembly and micro/nanodevice fabrication. *Adv. Mater.* **24**, 5284–5318 (2012).
11. X. Liang, B. A. Sperling, I. Calizo, G. Cheng, C. A. Hacker, Q. Zhang, Y. Obeng, K. Yan, H. Peng, Q. Li, X. Zhu, H. Yuan, A. R. Hight Walker, Z. Liu, L.-m. Peng, C. A. Richter, Toward clean and crackless transfer of graphene. *ACS Nano* **5**, 9144–9153 (2011).
12. Z. Yan, T. Pan, M. Xue, C. Chen, Y. Cui, G. Yao, L. Huang, F. Liao, W. Jing, H. Zhang, M. Gao, D. Guo, Y. Xia, Y. Lin, Thermal release transfer printing for stretchable conformal bioelectronics. *Adv. Sci.* **4**, 1700251 (2017).
13. S. Baik, D. W. Kim, Y. Park, T. J. Lee, S. Ho Bhang, C. Pang, A wet-tolerant adhesive patch inspired by protuberances in suction cups of octopi. *Nature* **546**, 396–400 (2017).
14. H. Lee, D.-S. Um, Y. Lee, S. Lim, H.-J. Kim, H. Ko, Octopus-inspired smart adhesive pads for transfer printing of semiconducting nanomembranes. *Adv. Mater.* **28**, 7457–7465 (2016).
15. M. K. Choi, O. K. Park, C. Choi, S. Qiao, R. Ghaffari, J. Kim, D. J. Lee, M. Kim, W. Hyun, S. J. Kim, H. J. Hwang, S.-H. Kwon, T. Hyeon, N. Lu, D.-H. Kim, Cephalopod-inspired miniaturized suction cups for smart medical skin. *Adv. Healthc. Mater.* **5**, 80–87 (2016).
16. W. M. Kier, A. M. Smith, The structure and adhesive mechanism of octopus suckers. *Integr. Comp. Biol.* **42**, 1146–1153 (2002).
17. F. Tramacere, L. Beccai, M. Kuba, A. Gozzi, A. Bifone, B. Mazzolai, The morphology and adhesion mechanism of *Octopus vulgaris* Suckers. *PLOS ONE* **8**, e65074 (2013).
18. J. Kim, Y. Cho, S. Kim, J. Lee, 3D cocontinuous composites of hydrophilic and hydrophobic soft materials: High modulus and fast actuation time. *ACS Macro Lett.* **6**, 1119–1123 (2017).
19. H. Bai, A. Polini, B. Delattre, A. P. Tomsia, Thermoresponsive composite hydrogels with aligned macroporous structure by ice-templated assembly. *Chem. Mater.* **25**, 4551–4556 (2013).
20. P. Gao, P. R. Nixon, J. W. Skoug, Diffusion in HPMC gels. II. Prediction of drug release rates from hydrophilic matrix extended-release dosage forms. *Pharm. Res.* **12**, 965–971 (1995).
21. D. Wirthl, R. Pichler, M. Drack, G. Kettlguber, R. Moser, R. Gerstmayr, F. Hartmann, E. Bradt, R. Kaltseis, C. M. Siket, S. E. Schausberger, S. Hild, S. Bauer, M. Kaltenbrunner, Instant tough bonding of hydrogels for soft machines and electronics. *Sci. Adv.* **3**, e1700053 (2017).
22. N. Tananuvat, K. Bumroongkit, C. Tocharusa, U. Mevatee, A. Kongkaew, S. Ausayakhun, Limbal stem cell and oral mucosal epithelial transplantation from ex vivo cultivation in LSCD-induced rabbits: Histology and immunologic study of the transplant epithelial sheet. *Int. Ophthalmol.* **37**, 1289–1298 (2017).
23. P. Prabhasawat, P. Ekpo, M. Uiprasertkul, S. Chotikavanich, N. Tesavibul, K. Pornpanich, P. Luemsamran, Long-term result of autologous cultivated oral mucosal epithelial transplantation for severe ocular surface disease. *Cell Tissue Bank.* **17**, 491–503 (2016).
24. S. Han, M. K. Kim, B. Wang, D. S. Wie, S. Wang, C. H. Lee, Mechanically reinforced skin-electronics with networked nanocomposite elastomer. *Adv. Mater.* **28**, 10257–10265 (2016).
25. J.-W. Jeong, M. K. Kim, H. Cheng, W.-H. Yeo, X. Huang, Y. Liu, Y. Zhang, Y. Huang, J. A. Rogers, Capacitive epidermal electronics for electrically safe, long-term electrophysiological measurements. *Adv. Healthc. Mater.* **3**, 642–648 (2014).
26. Z. Wang, L. Millet, M. Mir, H. Ding, S. Unarunotai, J. Rogers, M. U. Gillette, G. Popescu, Spatial light interference microscopy (SLIM). *Opt. Express* **19**, 1016–1026 (2011).

Acknowledgments
Funding: This work was supported by the National Science Foundation (STC-EBICS grant nos. CBET-0939511 and CBET-1932192), the National Institutes of Health (1R21 HL109192), the Department of Defense Vision Research Program under Award (W81XWH-17-1-022), and the Jump ARCHES endowment through the Health Care Engineering Systems Center at University of Illinois at Urbana-Champaign and partly by Korea Institute of Science and Technology-Europe. C.H.L. is funded by the NIH National Institute of Biomedical Imaging and Bioengineering (NIBIB: 1R21EB026099-01A1). E.E.H. acknowledges the financial support from the University of Illinois' Beckman Institute Graduate Fellowship. H.C. and N.M. gratefully acknowledge funding support from the National Science Foundation under award no. 1554249 and the International Institute for Carbon Neutral Energy Research (WPI-I2CNER), sponsored by the Japanese Ministry of Education, Culture, Sports, Science and Technology. V.K.A. acknowledges financial support from National Institutes of Health, National Eye Institute K08 EY024339 and R01EY029409; Department of Defense, Congressionally Directed Medical Research Program, Vision Research Program W81XWH-17-1-0122 (V.K.A. and H.K.); Veterans Affairs Office of Research and Development I01BX004080; Unrestricted Grant from Research to Prevent Blindness, New York; and National Institutes of Health, National Eye Institute P30 EY001792. **Author contributions:** B.S.K. and H.K. designed this project and wrote the manuscript. M.K.K., Y.P., and C.H.L. developed the flexible heater and performed the electrophysiology recordings. Y.C. and S.G.I. supported the cell sheet preparation. E.E.H. and M.U.G. performed and analyzed animal experiments. H.C. and N.M. helped to investigate electrothermal actuation of the gel. K.M.S. and L.B.S. supported and advised on animal experiments. V.K.A., K.K., and K.-N.S. advised on the tissue transplantation. C.H. and G.P. performed SLIM observation of the cell sheet, W.C.B. and S.Y. performed adhesion tests, B.S.K. performed all other experiments. J.L., C.H.L., and H.K. supervised the project. All authors discussed the results and contributed to the final version of the manuscript. **Competing interests:** H.K., B.S.K., C.H.L., J.L., and M.K.K. are inventors on a provisional patent application related to this work filed by the University of Illinois at Urbana-Champaign, Purdue University, and Chung Ang University (filed on 31 August 2020; no. 63/072,634). The authors declare no other competing interests. **Data and materials availability:** All data needed to evaluate the conclusions in the paper are present in the paper and/or the Supplementary Materials. Additional data related to this paper may be requested from the authors.

Submitted 1 May 2020
Accepted 1 September 2020
Published 16 October 2020
10.1126/sciadv.abc5630

Citation: B. S. Kim, M. K. Kim, Y. Cho, E. E. Hamed, M. U. Gillette, H. Cha, N. Miljkovic, V. K. Aakalu, K. Kang, K.-N. Son, K. M. Schachtschneider, L. B. Schook, C. Hu, G. Popescu, Y. Park, W. C. Ballance, S. Yu, S. G. Im, J. Lee, C. H. Lee, H. Kong, Electrothermal soft manipulator enabling safe transport and handling of thin cell/tissue sheets and bioelectronic devices. *Sci. Adv.* **6**, eabc5630 (2020).

ScienceAdvances

Electrothermal soft manipulator enabling safe transport and handling of thin cell/tissue sheets and bioelectronic devices

Byoung Soo Kim, Min Ku Kim, Younghak Cho, Eman E. Hamed, Martha U. Gillette, Hyeongyun Cha, Nenad Miljkovic, Vinay K. Aakalu, Kai Kang, Kyung-No Son, Kyle M. Schachtschneider, Lawrence B. Schook, Chenfei Hu, Gabriel Popescu, Yeonsoo Park, William C. Ballance, Seunggun Yu, Sung Gap Im, Jonghwi Lee, Chi Hwan Lee and Hyunjoon Kong

Sci Adv **6** (42), eabc5630.
DOI: 10.1126/sciadv.abc5630